Electric polarization near vortices in the extended Kitaev model

Lucas R. D. Freitas,[1,2] Tim Bauer,[2,1] Reinhold Egger,[2] and Rodrigo G. Pereira[1]

[1] *International Institute of Physics and Departamento de Física Teórica e Experimental, Universidade Federal do Rio Grande do Norte, Natal, RN, 59078-970, Brazil*

[2] *Institut für Theoretische Physik, Heinrich-Heine-Universität, D-40225 Düsseldorf, Germany*

to be written

I. INTRODUCTION

A hallmark of Kitaev spin liquids is the fractionalization of spin-1/2 local moments into Majorana fermions and a $\mathbb{Z}_2$ gauge field [1–6]. When time reversal symmetry is broken by an external magnetic field, both types of excitations become gapped, and vortices of the $\mathbb{Z}_2$ gauge field bind Majorana zero modes that behave as non-Abelian anyons. These properties can be demonstrated in the exactly solvable Kitaev honeycomb model [1]. Since the observation that the bond-directional exchange interactions of the pure Kitaev model are realized in quasi-two-dimensional Mott insulators with strong spin-orbit coupling [7], identifying signatures of fractional excitations in Kitaev materials has become a major goal of condensed matter physics [8–11]. Most notably, there is evidence for a half-quantized thermal Hall conductance in the candidate material α-$RuCl_3$ at intermediate temperatures and magnetic fields, but its interpretation in terms of chiral Majorana edge modes remains controversial [12–15]. This ambiguity calls for alternative experimental probes that may help distinguish a Kitaev spin liquid from a more conventional partially polarized phase with topological magnons [16, 17].

A promising route to detect and manipulate the fractional excitations of Kitaev spin liquids is to exploit their nontrivial responses to electrical probes. Theoretical proposals in this direction include scanning tunneling spectroscopy [18–22], interferometry in electrical conductance [23, 24], and electric polarization and orbital currents associated with localized excitations [25, 26]. In fact, the charge polarization in Mott insulators can be captured by an effective density operator written in terms of spin correlations in the low-energy sector [27, 28]. The effective density operator for Kitaev materials was derived in Ref. [25] starting from the multi-orbital Hubbard-Kanamori model in the ideal limit where the dominant exchange path only generates the pure Kitaev interaction [7]. The electric field effects then work both ways. On the one hand, the inhomogeneous spin correlations around a $\mathbb{Z}_2$ vortex imply that vortices produce an intrinsic electric charge distribution. On the other hand, vortices are attracted by electrostatic potentials that locally modify exchange couplings, and this effect can be used to trap and move anyons adiabatically [25, 29].

In this work we generalize the theory of the electric charge response in Ref. [25] to consider the generic spin model for Kitaev materials [30]. Our starting point is the three-orbital Hubbard-Kanamori model that takes into account sub-dominant hopping processes that, in addition to Kitaev (K) interactions, also generate Heisenberg (J) and off-diagonal (Γ) exchange interactions. Using perturbation theory to leading order in the hopping parameters, we derive an expression for the effective charge density operator in the Mott insulating phase that contains all two-spin terms allowed by symmetry. Since the additional interactions spoil the integrability of the pure Kitaev model, we compute spin correlations using a Majorana mean-field theory. This type of approximation has been applied to map out the ground state phase diagram and compute response functions of the extended Kitaev model [31–39]. Here we generalize the mean-field approach to treat position-dependent order parameters in the case where translation symmetry is broken by the presence of vortices in the $\mathbb{Z}_2$ flux configuration. Including a Zeeman coupling, we show that the spatial anisotropy of the charge distribution around a vortex varies with the direction of the magnetic field and can be quantified by the components of the electric quadrupole moment. We also discuss how a local electrostatic potential renormalizes the couplings in the extended Kitaev model and gives rise to an effective attractive potential for vortices... finalize at the end

This paper is organized as follows. In Sec. II we introduce the Hubbard-Kanamori model and review the derivation of the extended Kitaev model... finalize at the end

II. MODEL

The local degrees of freedom of Kitaev materials are transition metal ions with $4d^5$ or $5d^5$ electronic configuration and strong spin-orbit coupling [2, 3]. In the presence of the crystal field of an octahedral ligand cage, this configuration is equivalent to a single hole in a t_{2g} orbital. We denote by $h^\dagger_{i\alpha\sigma}$ the operator that creates a hole at site i with spin $\sigma \in \{\uparrow,\downarrow\}$ and orbital $\alpha = x, y, z$ for the three t_{2g} orbitals yz, xz, xy, respectively.

The three-orbital Hubbard-Kanamori Hamiltonian on the honeycomb lattice has the form [30]

$$H_{\rm HK} = V + H_{\rm so} + T. \tag{1}$$

The first term contains the on-site interactions, given by

$$V = \sum_i \left[\frac{U - 3J_H}{2} (\bar{N}_i - 1)^2 - 2J_H \mathbf{S}_i^2 - \frac{J_H}{2} \mathbf{L}_i^2 \right], \tag{2}$$

where U is the repulsive interaction strength, J_H is Hund's coupling, and the operators $\bar{N}_i$, $\mathbf{S}_i$ and $\mathbf{L}_i$ are the total number, spin and orbital angular momentum of holes at site i. Defining the spinor $h_i^\dagger = (h_{ix\uparrow}^\dagger, h_{iy\uparrow}^\dagger, h_{iz\uparrow}^\dagger, h_{ix\downarrow}^\dagger, h_{iy\downarrow}^\dagger, h_{iz\downarrow}^\dagger)$, we write

$$\bar{N}_i = h_i^\dagger h_i, \quad \mathbf{S}_i = \frac{1}{2} h_i^\dagger (\boldsymbol{\sigma} \otimes \mathbb{1}_3) h_i, \quad \mathbf{L}_i = h_i^\dagger (\mathbb{1}_2 \otimes \mathbf{l}) h_i, \tag{3}$$

where $\boldsymbol{\sigma}$ is the vector of Pauli matrices acting in spin space and $\mathbf{l} = (l_x, l_y, l_z)$ is a vector of 3×3 matrices that represent the effective $l = 1$ angular momentum of the t_{2g} states [25]. The spin-orbit coupling term

$$H_{\rm so} = \lambda \sum_i \sum_{\alpha=x,y,z} h_i^\dagger (\sigma^\alpha \otimes l^\alpha) h_i \tag{4}$$

splits the degeneracy of the t_{2g} manifold. At each site the low-energy subspace is spanned by the states

$$\begin{aligned} |+\rangle &= \frac{1}{\sqrt{3}} \left(-|z,\uparrow\rangle - i\,|y,\downarrow\rangle - |x,\downarrow\rangle \right), \\ |-\rangle &= \frac{1}{\sqrt{3}} \left(|z,\downarrow\rangle + i\,|y,\uparrow\rangle - |x,\uparrow\rangle \right), \end{aligned} \tag{5}$$

which are associated with total angular momentum $j_{\rm eff} = \frac{1}{2}$. Finally, the hopping term in Eq. (1) has the form

$$T = -\sum_{ij} h_i^\dagger \left(\mathbb{1}_2 \otimes \mathbf{T}_{ij} \right) h_j. \tag{6}$$

The hopping matrix $\mathbf{T}_{ij}$ in orbital space depends on the orientation of the bond between sites i and j. We label the bonds on the honeycomb lattice by $\gamma \in \{x, y, z\} \equiv \{1, 2, 3\}$ corresponding to nearest-neighbor vectors $\boldsymbol{\delta}_x = \frac{1}{2}\hat{\mathbf{a}} + \frac{1}{2\sqrt{3}}\hat{\mathbf{b}}$, $\boldsymbol{\delta}_y = -\frac{1}{2}\hat{\mathbf{a}} + \frac{1}{2\sqrt{3}}\hat{\mathbf{b}}$, and $\boldsymbol{\delta}_z = -\frac{1}{\sqrt{3}}\hat{\mathbf{b}}$, respectively. Here $\hat{\mathbf{a}} = (1, 1, -2)/\sqrt{6}$ and $\hat{\mathbf{b}} = (-1, 1, 0)/\sqrt{2}$ are unit vectors in the honeycomb plane, with coordinates specified in terms of the crystallographic axes $\hat{\mathbf{x}}$, $\hat{\mathbf{y}}$ and $\hat{\mathbf{z}}$ of the ligand octahedra. We parametrize the hopping matrix for a nearest-neighbor z bond as [30]

$$\mathbf{T}_{\langle ij \rangle_z} = \begin{pmatrix} t_1 & t_2 & t_4 \\ t_2 & t_1 & t_4 \\ t_4 & t_4 & t_3 \end{pmatrix}. \tag{7}$$

The hopping matrix for x and y bonds can be obtained from Eq. (7) by a cyclic permutation of the orbital indices. Microscopically, the hopping parameters are associated with direct hopping between d orbitals or hoppings mediated by the ligand ions. Neglecting trigonal distortions, hereafter we set $t_4 = 0$ [3, 30].

The effective spin Hamiltonian for the Mott insulating phase can be derived by applying perturbation theory in the regime $U, J_H \gg \lambda \gg t_1, t_2, t_3$. We use the canonical transformation

$$\begin{aligned} \tilde{H}_{\rm HK} &= e^S H_{\rm HK} e^{-S} \\ &= H_{\rm HK} + [S, H_{\rm HK}] + \frac{1}{2}[S, [S, H_{\rm HK}]] + \cdots . \end{aligned} \tag{8}$$

The anti-Hermitian operator $S = \sum_{k=1}^\infty S_k$ is chosen so that S_k eliminates the terms that change the hole occupation numbers $\bar{N}_i$ at k-th order in the hopping parameters. For the calculation of the effective spin Hamiltonian, it suffices to consider the first-order term $S_1 = S_1^+ - S_1^-$, where $(S_1^-)^\dagger = S_1^+$ with

$$S_1^+ = \sum_{ij} \sum_\ell \frac{1}{\Delta E_\ell} \mathcal{P}_{i,\ell}^{(2)}\, h_i^\dagger (\mathbb{1} \otimes \mathbf{T}_{ij}) h_j\, \mathcal{P}_j^{(1)}. \tag{9}$$

Here $\mathcal{P}_i^{(1)}$ is a projector onto the subspace of a single hole at site i and $\mathcal{P}_{i,\ell}^{(2)}$ projects onto the subspace of two holes with total angular momentum $\ell \in \{0, 1, 2\}$. The excited states have energies ΔE_ℓ given by $\Delta E_0 = U + 2J_H$, $\Delta E_1 = U - 3J_H$, and $\Delta E_2 = U - J_H$. We then take

$$H = \mathcal{P}_{\rm low} \tilde{H}_{\rm HK} \mathcal{P}_{\rm low}, \tag{10}$$

where $\mathcal{P}_{\rm low} = \prod_i \left(|+_i\rangle \langle +_i| + |-_i\rangle \langle -_i| \right)$ is the projector onto the low-energy subspace restricted to $j_{\rm eff} = \frac{1}{2}$ states at every site. The result is the extended Kitaev model, also known as the $JK\Gamma$ model [30]:

$$H = \sum_{\langle ij \rangle_\gamma} \Big[J \boldsymbol{\sigma}_i \cdot \boldsymbol{\sigma}_j + K \sigma_i^\gamma \sigma_j^\gamma + \Gamma \big(\sigma_i^\alpha \sigma_j^\beta + \sigma_i^\beta \sigma_j^\alpha \big) \Big], \tag{11}$$

with an implicit sum over bond type $\gamma = x, y, z$ and α, β chosen so that $(\alpha\beta\gamma)$ is a cyclic permutation of (xyz). Here σ_i^γ denotes the γ component of the pseudospin-1/2 operator at site i. The couplings are

$$\begin{aligned} J = \frac{1}{27} \Bigg[&\frac{(2t_1 + t_3)^2}{U + 2J_H} + \frac{6t_1(t_1 + 2t_3)}{U - 3J_H} \\ &+ \frac{2(t_1 - t_3)^2}{U - J_H} \Bigg], \end{aligned} \tag{12}$$

$$K = \frac{2J_H}{9} \frac{(t_1 - t_3)^2 - 3t_2^2}{(U - 3J_H)(U - J_H)}, \tag{13}$$

$$\Gamma = \frac{4J_H}{9} \frac{t_2(t_1 - t_3)}{(U - 3J_H)(U - J_H)}. \tag{14}$$

In the limit $t_1, t_3 \to 0$ and $t_2 \neq 0$, the Hamiltonian in Eq. (11) reduces to the exactly solvable model with ferromagnetic Kitaev interactions [1]. This limit corresponds to a single hopping path mediated by ligands on edge-sharing octahedra with ideal 90° bonds [7]. Numerical studies show that the Kitaev spin liquid phase is stable in the regime $|\Gamma|, |J| \ll |K|$ [30, 40–42]. For estimates of the hopping and exchange parameters for α-$RuCl_3$, see for instance Refs. [3, 43]. In this material, one finds a ferromagnetic Kitaev coupling ($K < 0$), and the leading perturbation to the idealized Kitaev model is given by $0 < \Gamma < |K|$.

III. KITAEV SPIN LIQUID PHASE IN THE MEAN-FIELD APPROXIMATION

We now discuss a mean-field approximation that will allow us to calculate spin correlations for the extended

Kitaev model. We also use this approximation to verify the stability of the Kitaev spin liquid phase against integrability-breaking perturbations.

If we add a Zeeman coupling to an external magnetic field $\mathbf{h}$, the effective spin Hamiltonian can be cast in the compact form

$$H = \frac{1}{2}\sum_{ij}\sum_{\alpha\beta}\sigma_i^\alpha \mathbf{J}_{ij}^{\alpha\beta}\sigma_j^\beta - \sum_i \mathbf{h}\cdot\boldsymbol{\sigma}_i, \tag{15}$$

where i and j are nearest neighbors, the factor $1/2$ in the interaction comes from changing the sum over bonds to a sum over sites, and $\mathbf{J}_{ij}$ is the bond-dependent exchange matrix. For example, for nearest-neighbor z bonds we have

$$\mathbf{J}_{\langle ij\rangle_z} = \begin{pmatrix} J & \Gamma & 0 \\ \Gamma & J & 0 \\ 0 & 0 & J+K \end{pmatrix}. \tag{16}$$

The exchange matrices for other nearest-neighbor bonds follow from cyclic permutations of the spin and bond indices in $\mathbf{J}^{\alpha\beta}_{\langle ij\rangle_\gamma}$.

For $J = \Gamma = h = 0$, the model can be solved exactly [1] using the Kitaev representation $\sigma_i^\gamma = \mathrm{i}c_i^0 c_i^\gamma$ in terms of four Majorana fermions, which obey $(c_i^\mu)^\dagger = c_i^\mu$ and $\{c_i^\mu, c_j^\nu\} = 2\delta_{ij}\delta_{\mu\nu}$. Throughout this paper, we use

$$\mu,\nu,\rho \in \{0,1,2,3\} \tag{17}$$

to denote all four fermion flavors, in contrast with $\alpha,\beta,\gamma \in \{1,2,3\}$ for spatial indices only. Physical states must respect the local constraint $D_i = c_i^0 c_i^1 c_i^2 c_i^3 = +1$. The algebra of the spin operators can be satisfied using different representations [44]. It is convenient to write the Kitaev representation in terms of the vector $c_i = (c_i^0, c_i^1, c_i^2, c_i^3)^{\mathrm{T}}$ and the antisymmetric matrices N^γ defined by

$$\sigma_i^\gamma = \frac{\mathrm{i}}{2}c_i^{\mathrm{T}}\mathrm{N}^\gamma c_i = \frac{\mathrm{i}}{2}\left(c_i^0 c_i^\gamma - c_i^\gamma c_i^0\right). \tag{18}$$

In addition, instead of imposing $D_i = +1$, we use the equivalent constraint [45]

$$c_i^{\mathrm{T}}\mathrm{G}^\gamma c_i = c_i^0 c_i^\gamma - c_i^\gamma c_i^0 + \sum_{\alpha\beta}\epsilon^{\alpha\beta\gamma}c_i^\alpha c_i^\beta = 0. \tag{19}$$

RE: three constraints $\gamma = x, y, z$ instead of a single one. Redundancy should be mentioned. For a discussion of the properties of the matrices N^γ and G^γ, see Appendix A.

We rewrite the spin Hamiltonian as

$$\begin{aligned} H \;=\; & \frac{1}{8}\sum_{ij}\sum_{\alpha\beta}\mathrm{i}c_i^{\mathrm{T}}\mathrm{N}^\alpha c_i\, \mathbf{J}_{ij}^{\alpha\beta}\,\mathrm{i}c_j^{\mathrm{T}}\mathrm{N}^\beta c_j \\ & -\frac{1}{4}\sum_{i\gamma}\left[2h^\gamma \mathrm{i}c_i^{\mathrm{T}}\mathrm{N}^\gamma c_i - \lambda_i^\gamma \mathrm{i}c_i^{\mathrm{T}}\mathrm{G}^\gamma c_i\right]. \end{aligned} \tag{20}$$

Here we introduce Lagrangian multipliers λ_i^γ associated with the local constraint in Eq. (19) [36, 38]. We decouple the quartic terms using two types of real-valued mean-field parameters,

$$\mathrm{U}_{ij}^{\mu\nu} = \langle \mathrm{i}c_i^\mu c_j^\nu\rangle, \qquad \mathrm{V}_i^{\mu\nu} = \langle \mathrm{i}c_i^\mu c_i^\nu\rangle, \tag{21}$$

which obey $\mathrm{U}_{ij}^{\mu\nu} = -\mathrm{U}_{ji}^{\nu\mu}$ and $\mathrm{V}_i^{\mu\nu} = 2\mathrm{i}\delta^{\mu\nu} - \mathrm{V}_i^{\nu\mu}$. I think the factor 2 is wrong! For the exactly solvable Kitaev model, one finds that $\mathrm{U}_{ij}^{\mu\nu}$ is diagonal in the indices μ,ν. In particular, the components $\mathrm{U}_{ij}^{\gamma\gamma}$ are related to the static $\mathbb{Z}_2$ gauge field and take values $\mathrm{U}_{ij}^{\gamma\gamma} = \pm 1$ when i,j form a nearest-neighbor γ bond, and $\mathrm{U}_{ij}^{\gamma\gamma} = 0$ otherwise. Thus, $\mathrm{U}_{ij}^{\gamma\gamma}$ can be viewed as an "order parameter" for the Kitaev spin liquid phase. For comparison with the exact solution, we also define

$$W_p = \prod_{\langle ij\rangle_\gamma \in p}\mathrm{U}_{ij}^{\gamma\gamma}, \tag{22}$$

where p is a hexagonal plaquette and the site indices in $\mathrm{U}_{ij}^{\gamma\gamma}$ are such that i belongs to sublattice A and j to sublattice B. In the pure Kitaev model, W_p is identified with the gauge-invariant $\mathbb{Z}_2$ flux, and the ground state lies in the sector with $W_p = +1$ for all plaquettes. States with $W_p = -1$ at isolated plaquettes are associated with vortex excitations [1]. Besides the link variables $\mathrm{U}_{ij}^{\mu\nu}$, in the mean-field approach we also consider the on-site fermion bilinears $\mathrm{V}_i^{\mu\nu}$. It follows from the Kitaev representation that $\mathrm{V}_i^{0\gamma} = \langle\sigma_i^\gamma\rangle$. Moreover, the constraint in Eq. (19) implies $\mathrm{V}_i^{\alpha\beta} = -\mathrm{V}_i^{0\gamma}$ for $(\alpha\beta\gamma)$ a cyclic permutation of (xyz). Thus, there are only three independent components of $\mathrm{V}_i^{\mu\nu}$ at each site, and they are related to the local magnetization induced by the external magnetic field. In the limit $|h| \gg |K|, |J|, |\Gamma|$, we expect to encounter a partially polarized phase characterized by $\mathrm{V}_i^{\mu\nu} \neq 0$ while $\mathrm{U}_{ij}^{\mu\nu} = 0$ for all bonds.

The mean-field Hamiltonian reads

$$H_{\mathrm{MF}} = \sum_{ij}\frac{\mathrm{i}}{4}c_i^{\mathrm{T}}\mathrm{A}_{ij}c_j + \sum_i \frac{\mathrm{i}}{4}c_i^{\mathrm{T}}\mathrm{B}_i c_i - \mathrm{C}. \tag{23}$$

The first term on the right-hand side couples Majorana fermions on nearest-neighbor bonds $\langle ij\rangle_\gamma$, via the 4×4 bond-dependent matrix

$$\mathrm{A}_{ij} = 2\sum_{\alpha\beta}\mathbf{J}_{ij}^{\alpha\beta}\mathrm{N}^\alpha \mathrm{U}_{ij}\mathrm{N}^\beta. \tag{24}$$

The onsite term involves the matrix

$$\begin{aligned} \mathrm{B}_i = & \sum_{j\in\mathcal{V}_i}\sum_{\alpha\beta}\mathbf{J}_{ij}^{\alpha\beta}\mathrm{N}^\alpha \mathrm{tr}\left(\mathrm{V}_j^{\mathrm{T}}\mathrm{N}^\beta\right) \\ & + \sum_\gamma(\lambda_i^\gamma \mathrm{G}^\gamma - 2h^\gamma \mathrm{N}^\gamma), \end{aligned} \tag{25}$$

where $\mathcal{V}_i$ denotes the set of nearest neighbors of site i.

Finally, the constant term is

$$\mathrm{C} = \frac{1}{8}\sum_{ij}\sum_{\alpha\beta}\mathbf{J}_{ij}^{\alpha\beta}\Big[\mathrm{tr}\big(\mathrm{V}_i^{\mathrm{T}}\mathrm{N}^{\alpha}\big)\,\mathrm{tr}\big(\mathrm{V}_j^{\mathrm{T}}\mathrm{N}^{\beta}\big) + 2\,\mathrm{tr}\big(\mathrm{U}_{ij}^{\mathrm{T}}\mathrm{N}^{\alpha}\mathrm{U}_{ij}\mathrm{N}^{\beta}\big)\Big]\,. \tag{26}$$

We diagonalize the mean-field Hamiltonian using

$$c = \sqrt{2}\,\mathbb{U}\begin{pmatrix} d \\ d^{\dagger}\end{pmatrix}, \quad \mathbb{U} = \begin{pmatrix}\mathbb{U}_{<} & \mathbb{U}_{>}\end{pmatrix}, \tag{27}$$

where c is a vector defined from $8N$ Majorana fermions for N unit cells, $\mathbb{U}$ is a unitary transformation, and d is a $4N$-component vector of annihilation operators of complex fermions. The columns of $\mathbb{U}_{<(>)}$ correspond to the eigenvectors of the mean-field Hamiltonian with negative (positive) energy. The mean-field ground state is the state annihilated by all d operators, from which it follows that

$$\langle\, \mathrm{i}c_{\mathrm{I}}\, c_{\mathrm{J}}\,\rangle = \mathrm{i}\big(\mathbb{U}_{<}\mathbb{U}_{<}^{\dagger}\big)_{\mathrm{IJ}}\,, \tag{28}$$

where $\mathrm{I} = (i,\mu)$ and $\mathrm{J} = (j,\nu)$ combine site and fermion flavor indices. We obtain the mean-field parameters in Eq. (21) by setting i and j to be either nearest neighbors or the same site. Together with the mean-field Hamiltonian, Eq. (28) defines a set of self-consistency equations, which we then solve numerically. In this approach, we require that the constraint in Eq. (19) be satisfied on average in the mean-field ground state, $\langle c_i^{\mathrm{T}}\mathrm{G}^{\gamma}c_i\,\rangle = 0$. For zero magnetic field and in the absence of magnetic order, this condition is automatically satisfied since $\mathrm{V}_i^{0\gamma} = \mathrm{V}_i^{\alpha\beta} = 0$. To describe the Kitaev spin liquid phase at finite magnetic field, we tune the Lagrange multipliers λ_i^{γ} contained in B_i in order to minimize the violation of the constraint, as measured by $|\,\langle c_i^{\mathrm{T}}\mathrm{G}^{\gamma}c_i\,\rangle\,|$. [Do we need more information about this in an appendix? See Notes-Lagrange-Multiplier.pdf.]

Let us first describe the mean-field solution in the homogeneous case in the absence of vortices. If the ground state does not break spin rotation or lattice symmetries, as in the Kitaev spin liquid phase, the matrices $\mathrm{U}_{ij}^{\mu\nu}$ depend only on the bond type γ, and we set $\mathrm{U}_{ij}^{\mu\nu} = \mathrm{U}_{\gamma}^{\mu\nu}$ for bonds $\langle ij\rangle_{\gamma}$ with i in sublattice A and j in lattice B. Moreover, $\mathrm{V}_i^{\mu\nu} = \mathrm{V}^{\mu\nu}$ becomes a constant matrix. More generally, we can allow these parameters to vary with the sublattice within larger unit cells to describe magnetically ordered phases. We solve the self-consistency equations using a Fourier transform of the Majorana modes in the thermodynamic limit. We first verify that the mean-field approach recovers the exact result for the Kitaev model when we set $\Gamma = J = h = 0$. The dispersion relation of the Majorana fermions is depicted by dashed lines in Fig. 1. In this case, the only dispersive band is associated with the fermion c^0. This band is gapless with a Dirac spectrum near the K point. In addition, there are three degenerate flat bands associated with the fermions c^{γ}, which are related to the static gauge variables $\mathrm{U}_{\gamma}^{\gamma\gamma}$.

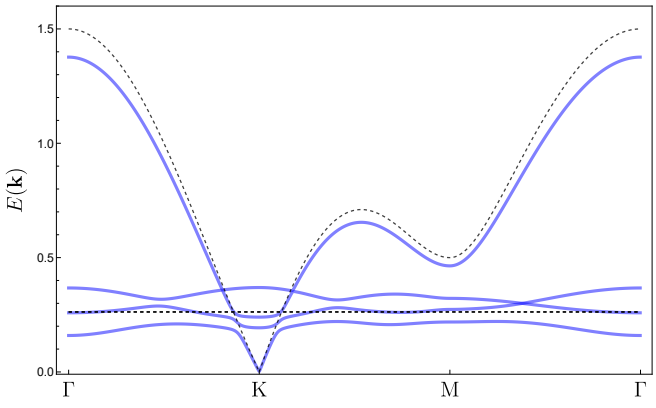

Figure 1. Dispersion relation of Majorana fermions calculated within the mean-field approach for the homogeneous system with $K = -1$, $J = 0$, $\Gamma = 0.20$, and $\mathbf{h} = 0.2\hat{\mathbf{c}}$. For comparison, the dashed lines show the dispersion in the pure Kitaev limit.

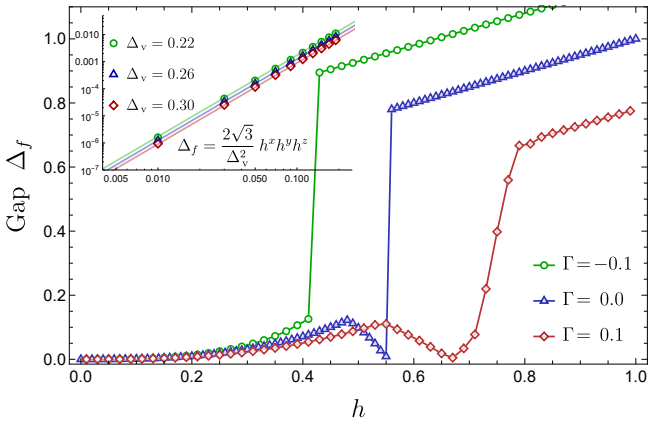

Figure 2. Fermion gap as a function of magnetic field for $\mathbf{h} = h\hat{\mathbf{c}}$ along the $\hat{\mathbf{c}}$ axis, with $K = -1$, $J = 0$, and for three values of Γ: $\Gamma = 0$ (blue circles) and $\Gamma = 0.2$ (red triangles). there are three values in the figure, and the symbols are different The inset shows that for weak fields the fermion gap agrees with the perturbative result to leading order in h; here the vison gap is $\Delta_v = 0.26$ for $\Gamma = 0$ and $\Delta_v = 0.30$ for $\Gamma = 0.1$. [Need to explain how Δ_v was calculated.] [$1/\Delta_v^2$ is obtained from a linear fit of $\Delta_f = \frac{2}{3\Delta_v}h^3$ in small h^3, note that here $h^x = h^z = h^z = h/\sqrt{3}$.]

Moving away from the exactly solvable point, we find that all bands become dispersive. For $h = 0$ and $K, \Gamma, J \neq 0$, we checked that our results are in quantitative agreement with a previous mean-field calculation [31]. Our approach also allows us to take into account the magnetic field nonperturbatively. In this case, we monitor the constraint in the mean-field solution and tune the uniform Lagrange multipliers λ^{γ} to ensure that

$|\langle c_i^{\rm T} {\rm G}^\gamma c_i \rangle| < 0.05$, which is much smaller than the maximum possible violation of the constraint, $|\langle c_i^{\rm T} {\rm G}^\gamma c_i \rangle| = 1$. [Explain analytical bound?] [I defined the constraint violation as the norm of the vector $|\langle c_i^{\rm T} {\rm G}^\gamma c_i \rangle|$ with normalization such that the upper bound is 1, which is $\frac{1}{4\sqrt{3}} \sqrt{\sum_\gamma \langle c_i^{\rm T} {\rm G}^\gamma c_i \rangle^2}$.]

Figure 1 shows the dispersion for a magnetic field pointing along the crystallographic c direction (perpendicular to the honeycomb plane), with unit vector $\hat{\mathbf{c}} = (1,1,1)/\sqrt{3}$. Clearly, the magnetic field opens up a gap in the fermion spectrum, as expected for the non-Abelian Kitaev spin liquid phase. As we increase the magnetic field, the gap at the K point increases, but the gap at the Γ point decreases. The fermion gap Δ_f is given by the minimum between the energies at the K and Γ points. If these energies cross, Δ_f exhibits a kink at the corresponding value of h; see the curve for $\Gamma = 0$ in Fig. 2. As we increase the magnetic field, we encounter a critical value h_c at which the gap either changes discontinuously, as in a first-order transition (e.g. $\Gamma = -0.1|K|$ in Fig. 2), or vanishes and varies continuously across the phase transition (e.g. $\Gamma = 0.1|K|$ in Fig. 2). Similar behavior has been obtained using a variational approach [46]. Note that adding $\Gamma > 0$ increases h_c, in qualitative agreement with exact diagonalization results [41]. However, in comparison with the latter, the mean-field approach overestimates the value of h_c for ferromagnetic Kitaev coupling [34, 41, 47, 48]. For $h \ll h_c$, we checked that the fermion gap behaves as $\Delta_f = 2\sqrt{3} h_x h_y h_z / \Delta_v^2$, where Δ_v is the vison gap, as expected from perturbation theory [1]. [Kitaev's expression is $\Delta_f = 6\sqrt{3}\kappa$ and the proportionality coefficient in $\kappa \sim h^3$ that I use comes from mean-field fit of the pure Kitaev limit.] For $\mathbf{h} = h\hat{\mathbf{c}}$, the fermion gap increases with the magnetic field as $\Delta_f \propto h^3$; see the inset in Fig. 2. As we vary the field direction, the gap closes when one component of $\mathbf{h}$ vanishes.

Δ_v has recently been computed exactly by Tsvelik. Cite and quote value?

We further assess the stability of the Kitaev spin liquid phase by evaluating the $\mathbb{Z}_2$ flux parameter in Eq. (22). In a homogeneous ground state, we have $W_p = ({\rm U}_\gamma^{\gamma\gamma})^6$. The result for the extended Kitaev model with $J = 0$ and $\Gamma, h \neq 0$ is shown in Fig. 3 for a magnetic field along the $\hat{\mathbf{c}}$ direction and for an in-plane field along the $\hat{\mathbf{a}}$ direction (perpendicular to the z bonds). As expected, $U_\gamma^{\gamma\gamma}$ decreases as we increase h or Γ. The dots in this figure mark the transition where the gap Δ_f vanishes continuously. Note that ${\rm U}_\gamma^{\gamma\gamma}$ varies smoothly across this transition for $\mathbf{h} \parallel \hat{\mathbf{c}}$ and $\Gamma > 0$. While for strong magnetic fields the system is in the partially polarized phase with uniform magnetization, the transition driven by increasing $\Gamma > 0$ is expected to be into a phase with vortex-type magnetic order [34, 49]. Here we do not explore the magnetic phases in detail, focusing instead on the regime of weak integrability-breaking perturbations where both ${\rm U}_\gamma^{\gamma\gamma}$ and Δ_f vary smoothly and take values comparable to those at the exactly solvable point. In this regime, we expect the mean-field approach to yield qualitatively correct results for the charge response of the Kitaev spin liquid phase.

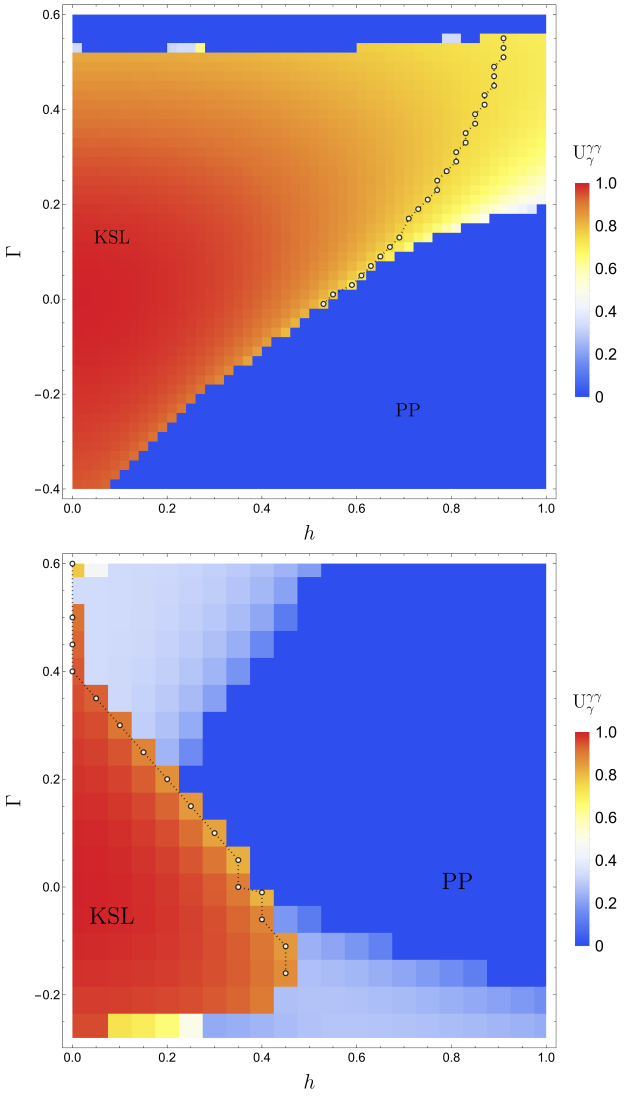

Figure 3. Mean-field phase diagram as a function of the magnetic field and Γ interaction for fixed $K = -1$ and $J = 0$. We show the result for two directions of the magnetic field: $\mathbf{h} \parallel \hat{\mathbf{c}}$, perpendicular to the honeycomb plane (top), and an in-plane field $\mathbf{h} \parallel \hat{\mathbf{a}}$ (bottom). The color scale represents the mean-field parameter ${\rm U}_\gamma^{\gamma\gamma}$, related to the $\mathbb{Z}_2$ flux W_p in Eq. (22) by $W_p = ({\rm U}_\gamma^{\gamma\gamma})^6$. White circles represent values where the gap closes at the Γ point.

IV. VORTEX CHARGE DENSITY PROFILE

Inhomogeneous spin correlations can bring on a charge redistribution in Mott insulators [27, 28]. In this section, we discuss the charge density profile induced by the presence of $\mathbb{Z}_2$ vortices in a Kitaev spin liquid. We first derive

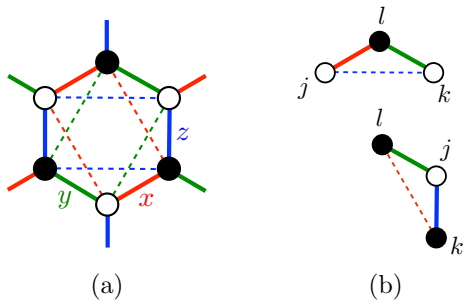

Figure 4. Honeycomb lattice with nearest- and next-nearest-neighbor hopping. (a) Red, green and blue lines correspond to $\gamma = x, y, z$ bonds, respectively. The hopping matrix on nearest-neighbor bonds (solid lines) is written in terms of hopping parameters t_1, t_2, t_3, and t_4; see Eq. (7). On second-neighbor bonds (dashed lines), we consider a single hopping parameter t_2'; see Eq. (30). (b) Examples of triangles that contribute to the effective charge density operator at site l.

the effective density operator in terms of two-spin operators and then proceed to calculate its expectation value using the Majorana mean-field approach.

Consider the hole density operator $\bar{N}_l$ at site l in the Hubbard-Kanamori model. Using the canonical transformation in Eq. (8), we can write the effective charge imbalance operator in the low-energy sector as

$$\delta n_l = \mathcal{P}_{\text{low}} e^{S} (\bar{N}_l - 1) e^{-S} \mathcal{P}_{\text{low}}. \tag{29}$$

We calculate δn_l using perturbation theory to leading order in the hopping matrix $\mathbf{T}_{ij}$. In systems with bond-inversion symmetry, like the Hubbard-Kanamori model in Eq. (1), the first non-vanishing contribution appears at third order and is associated with virtual processes in which an electron or hole moves around a triangle [25, 27, 28]. To obtain this leading contribution, we generalize the hopping matrix to include hopping between next-nearest-neighbor sites on the honeycomb lattice. We denote by $\langle\langle ij \rangle\rangle_\gamma$ a second-neighbor bond perpendicular to nearest-neighbor γ bonds, as shown in Fig. 4(a). Sizeable second- and third-neighbor hopping parameters have been calculated for Kitaev materials using *ab initio* methods [3, 43]. For simplicity, we consider only the dominant second-neighbor hopping, which on z bonds is described by the matrix

$$\mathbf{T}_{\langle\langle ij \rangle\rangle_z} = \begin{pmatrix} 0 & t_2' & 0 \\ t_2' & 0 & 0 \\ 0 & 0 & 0 \end{pmatrix}. \tag{30}$$

The second-neighbor hopping matrices on x and y bonds can be obtained by cyclic permutation of the indices. Assuming $|t_2'| \ll |t_1|, |t_2|, |t_3|$, we will calculate the charge density response to first order in t_2'. In this approximation, we neglect the second-neighbor exchange interaction generated by perturbation theory at order $(t_2')^2$, keeping only the nearest-neighbor exchange couplings as in Eq. (11).

Following Ref. [25], we write the effective charge imbalance operator as

$$\delta n_l = \sum_{(jk)} \delta n_{l,(jk)} \ , \tag{31}$$

where the sum over (jk) runs over pairs of sites such that jkl forms a triangle, and each triangle is counted once. These triangles contains two nearest-neighbor bonds and one next-nearest-neighbor bond; see the examples in Fig. 4(b). The calculation of δn_l requires the generator of the canonical transformation up to second order in the hopping matrices, $S \approx S_1 + S_2$. After the projection onto the $j_{\text{eff}} = \frac{1}{2}$ subspace, we write the end result in the form

$$\delta n_{l,(jk)} = \sum_{\alpha\beta} \left(\mathcal{C}_{jkl}^{\alpha 0 \beta} \sigma_j^\alpha \sigma_l^\beta + \mathcal{C}_{jkl}^{0 \alpha \beta} \sigma_k^\alpha \sigma_l^\beta + \mathcal{C}_{jkl}^{\alpha \beta 0} \sigma_j^\alpha \sigma_k^\beta \right). \tag{32}$$

Note that the effective density operator contains only two-spin operators because it must be invariant under time reversal. The coefficients $\mathcal{C}_{jkl}^{\mu\nu\rho}$ can be calculated as explained in Appendix B. We find closed-form but lengthy expressions for general values of the hopping parameters. For $t_1 = t_3 = 0$ and $t_2, t_2' \neq 0$, we recover the result of Ref. [25], in which the nonzero coefficients are diagonal in spin indices, e.g., $\mathcal{C}_{jkl}^{\alpha\beta 0} \sim \delta_{\alpha\beta} t_2^2 t_2' / U^3$. Similarly to the derivation of the effective Hamiltonian discussed in Sec. II, the addition of the subleading hopping parameters t_1 and t_3 generates off-diagonal terms in $\delta n_{l,(jk)}$ which are reminiscent of the Γ interaction.

Equation (32) implies that the charge density profile of a given state is determined by spin correlations. It follows from the charge neutrality of the Mott insulator, $\sum_l \langle \delta n_l \rangle = 0$, that there is no charge polarization in a homogeneous state where $\langle \delta n_l \rangle$ must be uniform. This condition is indeed satisfied when we impose that the spin correlations on different bonds respect translation and rotation symmetries, which provides a nontrivial check for the coefficients $\mathcal{C}_{jkl}^{\mu\nu\rho}$.

We now consider an inhomogeneous state in which translation symmetry is broken by the presence of vortices. In this case, we analyze the mean-field Hamiltonian on a finite system with linear size L along the directions of the primitive lattice vectors $\hat{\mathbf{e}}_1 = (\frac{1}{2}, \frac{\sqrt{3}}{2})$ and $\hat{\mathbf{e}}_2 = (-\frac{1}{2}, \frac{\sqrt{3}}{2})$, imposing periodic boundary conditions. To create vortices, we initialize the mean-field parameters in a configuration where we flip the sign of $\mathrm{U}_{ij}^{\mu\nu}$ on bonds crossed by open strings. In the pure Kitaev model, this procedure generates exact eigenstates with two localized vortices at the ends of the string. In the extended Kitaev model, vortices become mobile excitations with effective bandwidths governed by the integrability-breaking perturbations [50, 51]. In fact, for sufficiently large values of these perturbations, near the border of the Kitaev spin liquid phase in Fig. 3, we observe that the vortex positions vary as we iterate the self-consistency equations. When this happens, the string length decreases and the vortices move closer to each other until

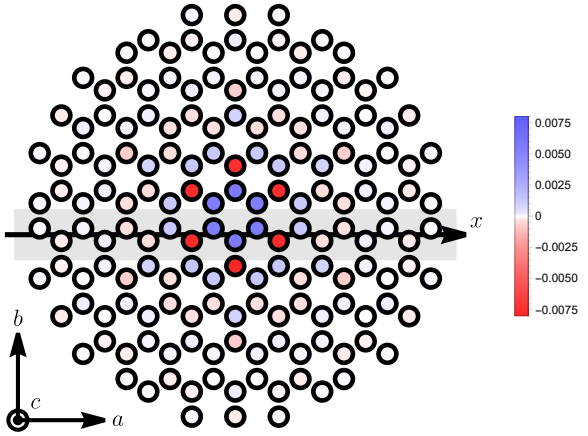

Figure 5. Charge imbalance $\langle \delta n_l \rangle$ in a state with a vortex located in the central hexagon. Here we fix the values of the coefficients $\mathcal{C}^{\mu\nu\rho}_{jkl}$ in Eq. (32) using the parameters of the Hubbard-Kanamori model $t_1 = 13$ meV, $t_2 = 160$ meV, $t_3 = -33$ meV, $t_2' = -60$ meV, $U = 2.6$ eV, and $J_H = 300$ meV. The values of δn_l are in units of $|t_2^2 t_2'/U^3| \approx 8.739 \times 10^{-5}$. The ratio between the exchange couplings calculated using Eq. (14) are $\Gamma/|K| = 0.20$ and $J/|K| = -0.02$. We set the magnetic field $\mathbf{h}/|K| = 0.2\mathbf{c}$. The solid line marks the zigzag path considered in Fig. 6.

.

they annihilate, and the mean-field solution converges to the vortex-free ground-state configuration. However, for $|\Gamma|, |J|, |h| \ll |K|$ and well separated vortices, we find a self-consistent solution with (metastable) localized vortices which corresponds to a local energy minimum in this sector of the Hilbert space. These results seem consistent with the real-time dynamics of vortices obtained within time-dependent mean-field theory [39]. Focusing on the regime of small perturbations, we can then compute static spin correlations near vortices using the position-dependent mean-field parameters $\mathrm{U}^{\mu\nu}_{ij}$ and $\mathrm{V}^{\mu\nu}_{i}$.

The charge imbalance profile in the vicinity of a vortex is shown in Fig. 5. The result from the mean-field approximation for the extended Kitaev model confirms the qualitative behavior obtained for the exactly solvable model in Ref. [25]. The charge imbalance oscillates between positive and negative values as we vary the distance from the center of the vortex, identified with the plaquette where $W_p < 0$. Moreover, as shown in Fig. 6, the magnitude of $\langle \delta n_l \rangle$ decays exponentially with the distance from the vortex, as expected due to the finite correlation length of the Kitaev spin liquid in a magnetic field. The value of $|\delta n_l|$ on sites around the vortex is of the order of 10^{-6}, producing local electric fields near the detection limit of state-of-the-art atomic force microscopy [25, 52, 53]. Importantly, here we use estimates for the hopping and interaction parameters for bulk α-$RuCl_3$, but the charge fluctuations can be greatly enhanced if the on-site repulsion U is screened in a monolayer by the interaction with a substrate.

Since the mean-field approach allows us to treat the Zeeman term nonperturbatively, we can go beyond the result of Ref. [25] and analyze the dependence of the charge redistribution on the field direction. For a field along the $\hat{\mathbf{c}}$ direction, the charge imbalance profile is isotropic around the position of the vortex, up to small variations due to the finite distance between vortices in the finite-size system. As we tilt the magnetic field on the ac plane (perpendicular to the z bonds), a small anisotropy develops in a way that the charge imbalance is enhanced in the direction perpendicular to the field. This effect can be seen in Fig. 6(b) as the difference between $\langle \delta n_l \rangle$ for the sites that belong to the hexagon that contains the vortex (three blue dots in the center; cf. Fig. 5).

We can quantify the anisotropy in the charge distribution by computing the electric multipole moments. In the limit of infinitely space vortices, the electric dipole vanishes because the system is invariant under spatial inversion about the vortex center. The first nontrivial multipole is the quadrupole moment, with components

$$Q_{\alpha\beta} = \sum_l \langle \delta n_l \rangle (3 R_{l\alpha} R_{l\beta} - |\mathbf{R}_l|^2 \delta_{\alpha\beta}). \tag{33}$$

Here $\alpha, \beta \in \{1, 2, 3\}$ and $\mathbf{R}_l = R_{l1}\hat{\mathbf{a}} + R_{l2}\hat{\mathbf{b}}$ (with $R_{l3} = 0$) is the position of site l with components given in terms of the in-plane unit vectors $\hat{\mathbf{a}}$ and $\hat{\mathbf{b}}$. Due to the finite system size, we calculate the quadrupole moment by summing over sites within a finite radius so that the sites considered are closer to the central vortex than to any other vortex. For a magnetic field along the $\hat{\mathbf{c}}$ direction, the rotational symmetry implies that the quadrupole tensor is diagonal and $Q_{11} = Q_{22} = -Q_{33}/2$. As we vary the field direction, the anisotropy is manifested in the off-diagonal elements and in the difference between Q_{11} and Q_{22}.

In Fig. 7 we show the angular dependence of the quadrupole components Q_{33}, $Q_{11} - Q_{22}$ and Q_{12} for the pure Kitaev model ($J = \Gamma = 0$) in a magnetic field. The component Q_{33} is maximum for a field along the $\hat{\mathbf{c}}$ direction, which may be interesting to maximize the intrinsic electric field produced at positions right above the vortex. Note that Q_{33} does not change sign, but varies around an average value with an angular dependence qualitatively similar to $|h_x h_y h_z|$. On the other hand, the difference $Q_{11} - Q_{22}$ vanishes for $\mathbf{h} \parallel \hat{\mathbf{c}}$, but is maximum when the field points along the $\hat{\mathbf{z}}$ axis. Note, however, that $|Q_{11} - Q_{22}|$ is one order of magnitude smaller than $|Q_{33}|$. Finally, Q_{12} vanishes if we tilt the field along the high-symmetry ac plane, but becomes nonzero for more general field directions.

Discuss h dependence in Fig. 8. [Can we get an exponent for $Q_{11} - Q_{22}$?]

[Vortex-vortex interactions?]

Stopped here...

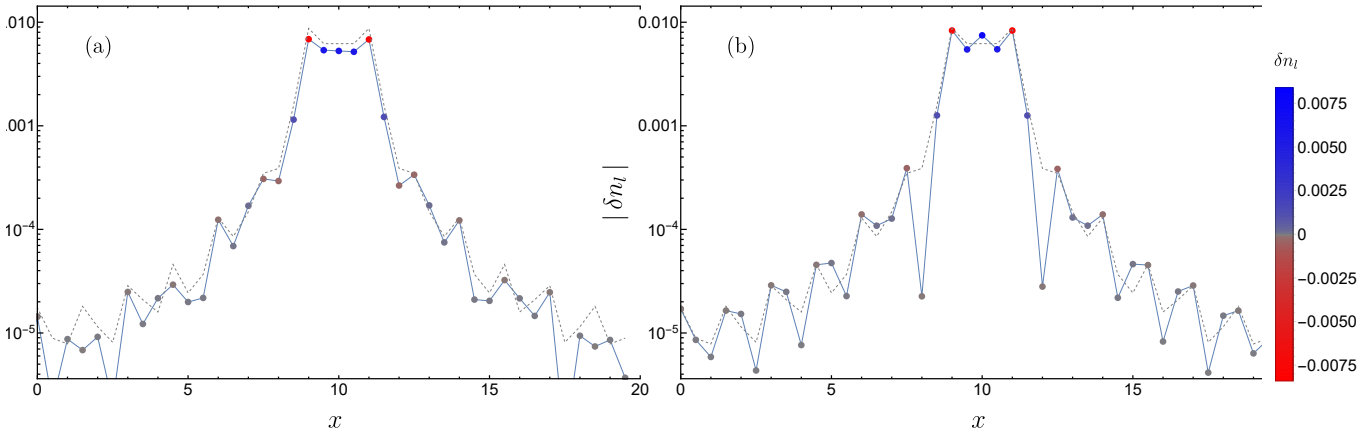

Figure 6. Magnitude of the charge imbalance as a function of the position along the zigzag path represented by the black line in Fig. 5. Here we used a lattice with linear size $L = 20$. The dots (connected by solid lines to guide the eye) correspond to the extended Kitaev model with exchange couplings $\Gamma/|K| = 0.20$ and $J/|K| = -0.02$. In addition, we set $|\mathbf{h}| = 0.3$ and consider two field directions: (a) $\mathbf{h} \parallel \mathbf{c}$, and (b) $\mathbf{h} \parallel \mathbf{z}$. For comparison, the dashed lines represent the result for the pure Kitaev model. [With κ instead of h?] [Pure Kitaev with $h = \kappa = 0$.]

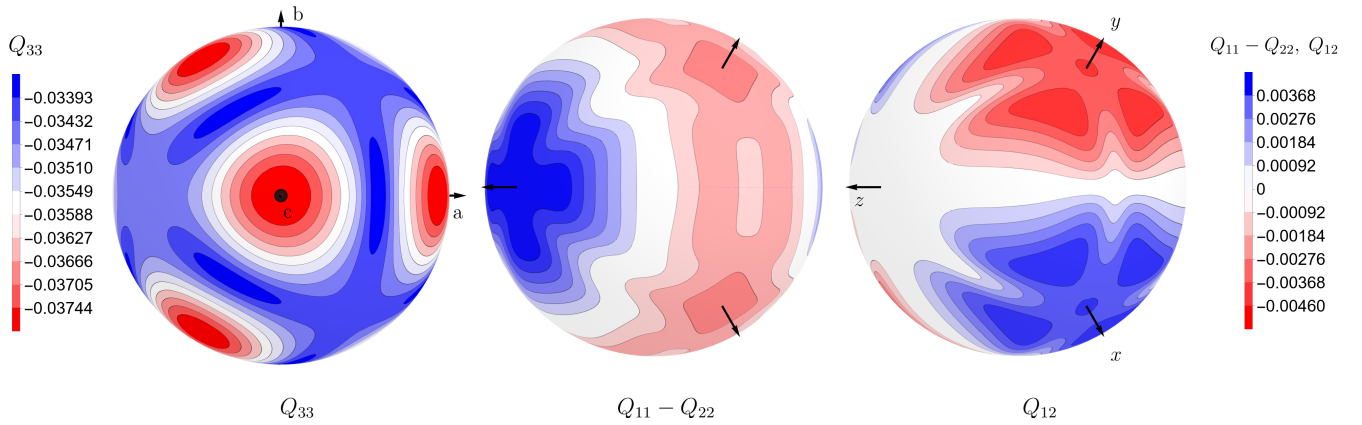

Figure 7. Calculation in the pure Kitaev model with second and third order perturbation theory in $\mathbf{h}$ for the quadrupole components as a function of magnetic field direction for $|\mathbf{h}| = 0.2$. [What does this mean exactly? Did you use the exactly solvable model with κ?] The scale is in units of $t_2^2 t_2'/U^3$. Q_{33} behaves as $|\kappa| \sim |h_x h_y h_z|$ while the anisotropy $Q_{11} - Q_{22}$ and the off diagonal term Q_{12} has a quadratic dependence according to the second order effect (h_x^2, h_y^2, h_z^2). [How do we understand this dependence?]

V. ELECTRICAL MANIPULATION

The mean field allows us to go beyond the uniform coupling limit. Here we consider the effect of applying an external electrical potential locally above a hexagonal plaquette. Changing the potential in the microscopic Hamiltonian to include the ultra local electric potential $\sum_{i\in\partial p} eV_0 N_i$ summing over the site on the boundary of a given plaquette p. Redoing the second order perturbation theory calculation with the inclusion of this potential, the effective Hamiltonian is of the same form as (11) but with bond dependent couplings for the bonds exterior to the

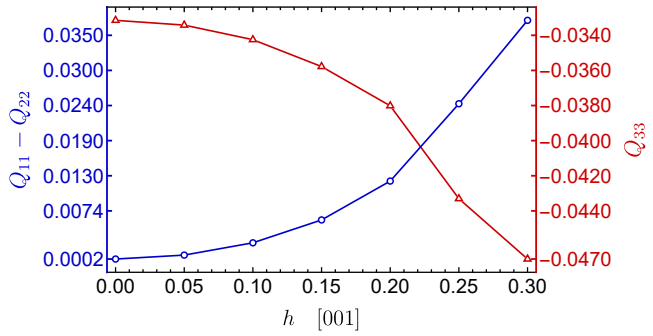

Figure 8. Quadrupole components Q_{33} and $Q_{11}-Q_{22}$ dependence in the magnetic field for z = [001] direction . [The anisotropy is maximum for the [001] direction]. Fixed $\Gamma/|K| = 0.14$. In units of $t_2^2 t_2'/U^3$. Comparing with Fig 7 the quadrupole magnitude is enhanced for positive Γ. [The crossing might be confusing. Plot $Q_{11}-Q_{22}$ and $-Q_{33}$ on the same scale; label curves using plot legends as in Fig. 2. Why aren't the tick marks on the vertical axis equally spaced? The axis should start from zero, not 0.0002.]

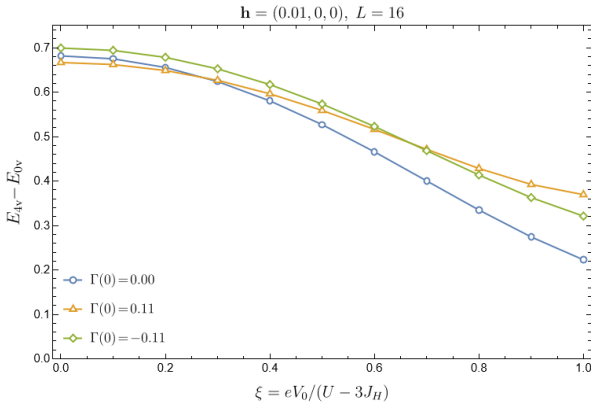

Figure 9. Vison gap dependence on applied electrostatic potential for different values of Γ in the FM $K < 0$ case. Gap increase for large field independent on the sign of Γ.

hexagon p. The coupling changes to

$$J(V_0) = \frac{1}{27}\Big[\ \frac{(2t_1+t_3)^2}{U+2J_H}\frac{1}{1-\xi_0^2} + \frac{6t_1(t_1+2t_3)}{U-3J_H}\frac{1}{1-\xi_1^2} + \frac{2(t_1-t_3)^2}{U-J_H}\frac{1}{1-\xi_2^2}\ \Big] \tag{34}$$

$$K(V_0) = K(0)\ \frac{1+\xi_1\xi_2}{(1-\xi_1^2)(1-\xi_2^2)}\ , \tag{35}$$

$$\Gamma(V_0) = \Gamma(0)\ \frac{1+\xi_1\xi_2}{(1-\xi_1^2)(1-\xi_2^2)}\ . \tag{36}$$

where $\xi_\ell = eV_0/\Delta E_\ell$.

Discussion on the dependence of the vison gap on the electric potential, and that it does not close even for non-zero Γ ...

VI. CONCLUSION

ACKNOWLEDGMENTS

We acknowledge funding by the Brazilian ministries MEC and MCTI, by the Brazilian agency CNPq, and by the Coordenação de Aperfeiçoamento de Pessoal de Nível Superior - Brasil (CAPES), by the Deutsche Forschungsgemeinschaft (DFG, German Research Foundation), Projektnummer 277101999 - TRR 183 (project B04), Normalverfahren Projektnummer EG 96-13/1, and under Germany's Excellence Strategy - Cluster of Excellence Matter and Light for Quantum Computing (ML4Q) EXC 2004/1 - 390534769.

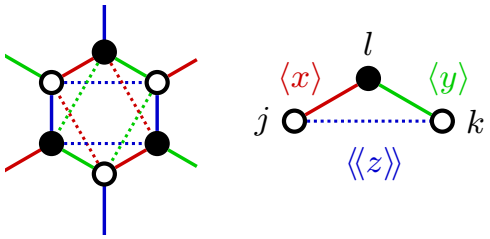

Figure 10.

Appendix A: Majorana representation

For each spin operator σ^γ we define four Majorana fermions c^μ, $\mu = 0, ..., 3$. The Majorana fermions are Hermitian and anti-commutes, which implies that we are making a $\mathfrak{su}(2)$ representation on the space of real and antisymmetric $\mathfrak{so}(4)$ matrices. As a basis of this space, we define the spin M^γ and isospin G^γ matrices following Ref. [45]

$$\mathrm{M}^1 = \sigma^3 \otimes \mathrm{i}\sigma^2,\ \mathrm{M}^2 = \mathrm{i}\sigma^2 \otimes \sigma^0,\ \mathrm{M}^3 = \sigma^1 \otimes \mathrm{i}\sigma^2, \tag{A1}$$

$$\mathrm{G}^1 = -\sigma^0 \otimes \mathrm{i}\sigma^2,\ \mathrm{G}^2 = -\mathrm{i}\sigma^2 \otimes \sigma^3,\ \mathrm{G}^3 = -\mathrm{i}\sigma^2 \otimes \sigma^1. \tag{A2}$$

They are real antissimetric matrices, $\mathrm{M}^\gamma, \mathrm{G}^\gamma \in \mathfrak{so}(4)$, satisfying the $\mathfrak{su}(2)$ spin algebra

$$[\mathrm{M}^\alpha, \mathrm{M}^\beta] = 2\varepsilon^{\alpha\beta\gamma}\mathrm{M}^\gamma, \quad [\mathrm{G}^\alpha, \mathrm{G}^\beta] = 2\varepsilon^{\alpha\beta\gamma}\mathrm{G}^\gamma, \tag{A3}$$

and commuting with each other $[\mathrm{M}^\alpha, \mathrm{G}^\beta] = 0$. These matrices are orthogonal $\left(\mathrm{M}^\alpha, \mathrm{G}^\beta\right) = 0$ with respect to the matrix inner product $(\mathrm{A}, \mathrm{B}) = \mathrm{tr}(\mathrm{A}^\mathrm{T}\mathrm{B}) = \sum_{\mu,\nu=0}^{3} \mathrm{A}^{\mu\nu}\mathrm{B}^{\mu\nu}$.

$$\left(\mathrm{M}^\alpha, \mathrm{M}^\beta\right) = 4\delta^{\alpha\beta}, \quad \left(\mathrm{G}^\alpha, \mathrm{G}^\beta\right) = 4\delta^{\alpha\beta}. \tag{A4}$$

On this framework, M^γ gives a natural representation for the spin projecting on the space orthogonal to G. However, for naturally recover the correct Kitaev model[1] as a limiting case on our mean-field, we will use the Kitaev representation (18)

$$\sigma_i^\gamma = \mathrm{i}c_i^0 c_i^\gamma = \frac{\mathrm{i}}{2} c_i^\mathrm{T} \mathrm{N}^\gamma c_i \ . \tag{A5}$$

In the basis of $\mathfrak{so}(4)$ matrices that we defined, this representation is $\mathrm{N}^\gamma = \frac{1}{2}\left(\mathrm{M}^\gamma - \mathrm{G}^\gamma\right)$ which does not satisfies the $\mathfrak{su}(2)$ Lie algebra itself, but the projective representation

$$[\sigma_i^\alpha, \sigma_j^\beta] = \mathrm{i}\delta_{ij}\varepsilon^{\alpha\beta\gamma}\left(2\sigma_j^\gamma + c_j^\mathrm{T}\mathrm{G}^\gamma c_j\right) \tag{A6}$$

Appendix B: Charge density coefficients

$$\delta n_l^{(3)} = -\mathcal{P}_{1\mathrm{h}} S_2^- \left[\delta n_l, S_1^+\right] \mathcal{P}_{1\mathrm{h}} + \mathrm{h.c.} \tag{B1}$$

Considering hopping over NN and NNN, the third-order contribution to the charge density at position l comes from sites jk that form a triangle with l. From now on let us drop the index (3). The charge imbalance at site l in third-order perturbation theory comes from a contribution that involves three sites as it can be written as

$$\delta n_l = \sum_{(jk)} \delta n_{l,(jk)} \ , \tag{B2}$$

where the sum over (jk) is a sum over all pairs of sites such that jkl forms a triangle. To avoid double counting, we consider only one pair in the sum $(jk) \equiv (kj)$, and the two contributions are already considered in $\delta n_{l,(jk)}$. To clear out the notation, I shall write

$$\delta n_{l,(jk)} = \delta n_{l,jk} + \delta n_{l,kj} \ . \tag{B3}$$

The matrix elements of the charge density for points in a triangle are

$$\begin{aligned}
&\langle s'_j, s'_k, s'_l|\delta n_l|s_j, s_k, s_l\rangle = \langle s'_j, s'_k, s'_l|\delta n_{l,jk}|s_j, s_k, s_l\rangle + \langle s'_j, s'_k, s'_l|\delta n_{l,kj}|s_j, s_k, s_l\rangle \\
&\langle s'_j, s'_k, s'_l|\delta n_{l,jk}|s_j, s_k, s_l\rangle = \\
&= -\sum_{s_2,s_3,s_4,s_5} \left(\mathbf{T}_{jk}\right)_{a'_j,a_2}\left(\mathbf{T}_{kl}\right)_{a_3,a_4}\left(\mathbf{T}_{lj}\right)_{a_5,a_j} \sum_{\ell,\ell'} \frac{F_{\ell'}(s'_k, s_2, s_3, s_k)\; F_{\ell}(s'_l, s_4, s_5, s_l)}{(\Delta E_\ell)^2\; \Delta E_{\ell'}} \\
&+ \sum_{s_2,s_3,s_4,s_5} \left(\mathbf{T}_{lk}\right)_{a'_j,a_2}\left(\mathbf{T}_{kj}\right)_{a_3,a_4}\left(\mathbf{T}_{jl}\right)_{a_5,a_l} \sum_{\ell,\ell'} \frac{F_{\ell}(s'_j, s_4, s_5, s_j)\; F_{\ell'}(s'_k, s_2, s_3, s_k)}{(\Delta E_\ell)^2\; \Delta E_{\ell'}} \\
&- \sum_{s_2,s_5} \left(\mathbf{T}_{jk}\right)_{a'_k,a_2}\left(\mathbf{T}_{kl}\right)_{a'_l,a_k}\left(\mathbf{T}_{lj}\right)_{a_5,a_l} \sum_{\ell} \frac{F_{\ell}(s'_j, s_2, s_5, s_j)}{(\Delta E_\ell)^3} \\
&+ \sum_{s_2,s_5} \left(\mathbf{T}_{lk}\right)_{a'_k,a_2}\left(\mathbf{T}_{kj}\right)_{a'_j,a_k}\left(\mathbf{T}_{jl}\right)_{a_5,a_j} \sum_{\ell} \frac{F_{\ell}(s'_l, s_2, s_5, s_l)}{(\Delta E_\ell)^3} + \text{h.c.}\,.
\end{aligned} \tag{B4}$$

where $F_\ell(s_1, s_2, s_3, s_4) = \langle s_1|h_{s_2}\; \mathcal{P}^{(2)}_\ell\; h^\dagger_{s_3}|s_4\rangle$ and ΔE_ℓ

After projecting in the $j_{\text{eff}} = 1/2$ subspace, the general expression for the charge density is

$$\delta n^{(3)}_{l,(jk)} = \sum_{\mu,\nu,\rho=0}^{3} \mathcal{C}^{\mu\nu\rho}_{jkl}\sigma^\mu_j\sigma^\nu_k\sigma^\rho_l\;, \quad \mathcal{C}^{\mu\nu\rho}_{jkl} = \frac{1}{8}\text{Tr}\left(\delta n^{(3)}_{l,(jk)}\,\sigma^\mu_j\sigma^\nu_k\sigma^\rho_l\right), \tag{B5}$$

where $\sigma^0 = \mathbb{1}$.

The charge density is even under time-reversal symmetry, thus only the terms with an even number of spins are non-zero. That is, for $\alpha, \beta, \gamma \in \{1, 2, 3\}$ we have

$$\mathcal{C}^{\alpha\beta\gamma}_{jkl} = 0\;, \quad \mathcal{C}^{\alpha 00}_{jkl} = 0\;, \quad \mathcal{C}^{0\alpha 0}_{jkl} = 0\;, \quad \mathcal{C}^{00\alpha}_{jkl} = 0\;. \tag{B6}$$

Then, the charge density can be written as

$$\delta n^{(3)}_{l,(jk)} = \sum_{\alpha\beta}\left(\mathcal{C}^{\alpha 0\beta}_{jkl}\sigma^\alpha_j\sigma^\beta_l + \mathcal{C}^{0\alpha\beta}_{jkl}\sigma^\alpha_k\sigma^\beta_l + \mathcal{C}^{\alpha\beta 0}_{jkl}\sigma^\alpha_j\sigma^\beta_k\right). \tag{B7}$$

For each s, there are three sets of 9 coefficients. To keep the expressions shorter, let us introduce the notation

$$\mathbb{C}^{\mu\nu\rho}_{(s)} = \frac{t_2^2\, t'_2}{U^3}\mathcal{C}^{\mu\nu\rho}_{(s)}\;, \quad \tau_i = t_i/t_2\;, \quad \eta = J_H/U\;. \tag{B8}$$

The coefficients are then:

$$\mathbb{C}^{110}_{(s=11)} = -\frac{\eta^2(2\eta-1)}{9(\eta-1)^3(3\eta-1)^3} \tag{B9}$$

$$\mathbb{C}^{120}_{(s=11)} = -\frac{\eta(\tau_1-\tau_3)\left[\left(276\eta^4-94\eta^2-6\eta+22\right)\tau_1+\left(26\eta^4-20\eta^3-7\eta^2-4\eta+5\right)\tau_3\right]}{54(\eta-1)^3(2\eta+1)^2(3\eta-1)^3} \tag{B10}$$

$$\mathbb{C}^{130}_{(s=11)} = \frac{\eta\left[\left(452\eta^4-8\eta^3-128\eta^2-46\eta+36\right)\tau_1+\left(454\eta^4-52\eta^3-175\eta^2+16\eta+45\right)\tau_3\right]}{108(\eta-1)^3(2\eta+1)^2(3\eta-1)^3} \tag{B11}$$

$$\mathbb{C}^{210}_{(s=11)} = -\frac{\eta(\tau_1-\tau_3)\left[\left(244\eta^4-16\eta^3-86\eta^2-2\eta+22\right)\tau_1+\left(58\eta^4-4\eta^3-15\eta^2-8\eta+5\right)\tau_3\right]}{54(\eta-1)^3(2\eta+1)^2(3\eta-1)^3} \tag{B12}$$

$$\mathbb{C}^{220}_{(s=11)} = -\frac{\eta^2(2\eta-1)}{9(\eta-1)^3(3\eta-1)^3} \tag{B13}$$

$$\mathbb{C}^{230}_{(s=11)} = \frac{\eta\left[\left(204\eta^4-24\eta^3-72\eta^2-2\eta+20\right)\tau_1+\left(98\eta^4+4\eta^3-29\eta^2-8\eta+7\right)\tau_3\right]}{36(\eta-1)^3(2\eta+1)^2(3\eta-1)^3} \tag{B14}$$

$$\mathbb{C}^{310}_{(s=11)} = \frac{\eta\left[\left(204\eta^4-24\eta^3-72\eta^2-2\eta+20\right)\tau_1+\left(98\eta^4+4\eta^3-29\eta^2-8\eta+7\right)\tau_3\right]}{36(\eta-1)^3(2\eta+1)^2(3\eta-1)^3} \tag{B15}$$

$$\mathbb{C}^{320}_{(s=11)} = \frac{\eta\left[\left(452\eta^4-8\eta^3-128\eta^2-46\eta+36\right)\tau_1+\left(454\eta^4-52\eta^3-175\eta^2+16\eta+45\right)\tau_3\right]}{108(\eta-1)^3(2\eta+1)^2(3\eta-1)^3} \tag{B16}$$

$$\mathbb{C}^{330}_{(s=11)} = -\frac{\eta\left(11\eta^2-10\eta+3\right)}{9(\eta-1)^3(3\eta-1)^3}\;, \tag{B17}$$

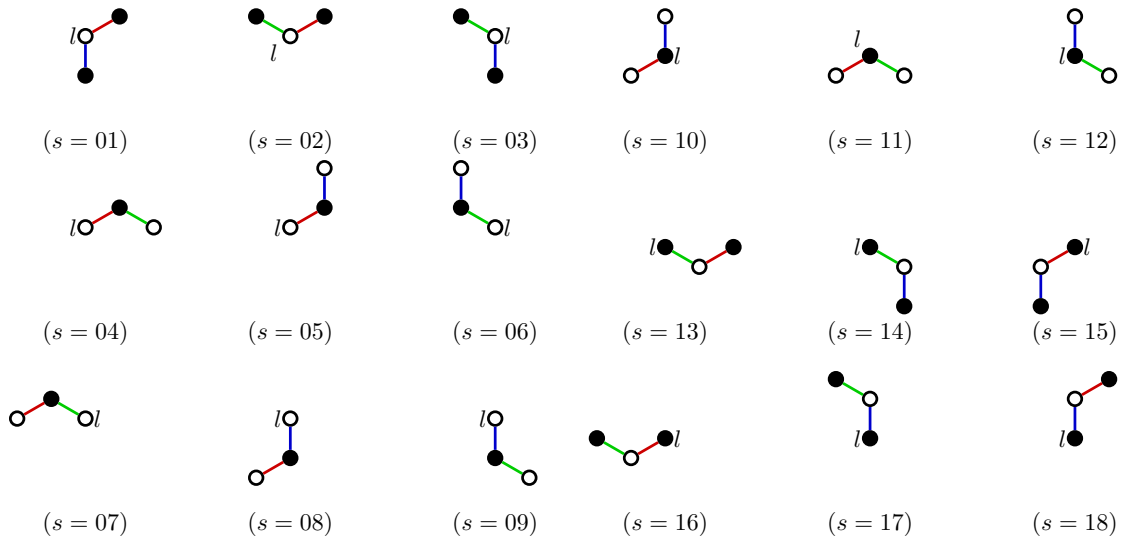

Figure 11. Triangles configurations. s = 01-09 are for the triangles where l is in the A sub-lattice, whereas for s = 10-18 l is in the B sublattice.

$$\mathbb{C}^{101}_{(s=11)} = \frac{\eta\left(11\eta^2-10\eta+3\right)}{18(\eta-1)^3(3\eta-1)^3} \tag{B18}$$

$$\mathbb{C}^{102}_{(s=11)} = -\frac{(\tau_1-\tau_3)\left[\left(514\eta^5+22\eta^4-287\eta^3+48\eta^2+33\eta-12\right)\tau_1+\left(91\eta^5+9\eta^4-63\eta^3+23\eta^2+6\eta-6\right)\tau_3\right]}{54(\eta-1)^3(2\eta+1)^2(3\eta-1)^3} \tag{B19}$$

$$\mathbb{C}^{103}_{(s=11)} = \frac{\eta\left[\left(116\eta^4+40\eta^3-72\eta^2+6\eta\right)\tau_1+\left(174\eta^4+12\eta^3-95\eta^2+8\eta+9\right)\tau_3\right]}{36(\eta-1)^3(2\eta+1)^2(3\eta-1)^3} \tag{B20}$$

$$\mathbb{C}^{201}_{(s=11)} = \frac{(\tau_1-\tau_3)\left[\left(102\eta^5-2\eta^4-65\eta^3+32\eta^2+11\eta-12\right)\tau_1+\left(245\eta^5-3\eta^4-126\eta^3+21\eta^2+19\eta-6\right)\tau_3\right]}{54(\eta-1)^3(2\eta+1)^2(3\eta-1)^3} \tag{B21}$$

$$\mathbb{C}^{202}_{(s=11)} = \frac{\eta\left(21\eta^2-20\eta+5\right)}{18(\eta-1)^3(3\eta-1)^3} \tag{B22}$$

$$\mathbb{C}^{203}_{(s=11)} = \frac{\left(252\eta^4-144\eta^3-90\eta^2+92\eta-24\right)\tau_1+\left(176\eta^4-81\eta^3-56\eta^2+49\eta-12\right)\tau_3}{108(\eta-1)^3(2\eta+1)(3\eta-1)^3} \tag{B23}$$

$$\mathbb{C}^{301}_{(s=11)} = \frac{\eta\left[\left(428\eta^4+88\eta^3-260\eta^2+38\eta+12\right)\tau_1+\left(442\eta^4+68\eta^3-241\eta^2+4\eta+15\right)\tau_3\right]}{108(\eta-1)^3(2\eta+1)^2(3\eta-1)^3} \tag{B24}$$

$$\mathbb{C}^{302}_{(s=11)} = -\frac{\left(388\eta^4-180\eta^3-118\eta^2+104\eta-24\right)\tau_1+\left(136\eta^4-45\eta^3-52\eta^2+37\eta-12\right)\tau_3}{108(\eta-1)^3(2\eta+1)(3\eta-1)^3} \tag{B25}$$

$$\mathbb{C}^{303}_{(s=11)} = -\frac{\eta\left(17\eta^2-18\eta+5\right)}{18(\eta-1)^3(3\eta-1)^3}\,, \tag{B26}$$

$$\mathbb{C}^{011}_{(s=11)} = \frac{\eta\left(21\eta^2-20\eta+5\right)}{18(\eta-1)^3(3\eta-1)^3} \tag{B27}$$

$$\mathbb{C}^{012}_{(s=11)} = \frac{(\tau_1-\tau_3)\left[\left(102\eta^5-2\eta^4-65\eta^3+32\eta^2+11\eta-12\right)\tau_1+\left(245\eta^5-3\eta^4-126\eta^3+21\eta^2+19\eta-6\right)\tau_3\right]}{54(\eta-1)^3(2\eta+1)^2(3\eta-1)^3} \tag{B28}$$

$$\mathbb{C}^{013}_{(s=11)} = \frac{\left(252\eta^4-144\eta^3-90\eta^2+92\eta-24\right)\tau_1+\left(176\eta^4-81\eta^3-56\eta^2+49\eta-12\right)\tau_3}{108(\eta-1)^3(2\eta+1)(3\eta-1)^3} \tag{B29}$$

$$\mathbb{C}^{021}_{(s=11)} = -\frac{(\tau_1-\tau_3)\left[\left(514\eta^5+22\eta^4-287\eta^3+48\eta^2+33\eta-12\right)\tau_1+\left(91\eta^5+9\eta^4-63\eta^3+23\eta^2+6\eta-6\right)\tau_3\right]}{54(\eta-1)^3(2\eta+1)^2(3\eta-1)^3} \tag{B30}$$

$$\mathbb{C}^{022}_{(s=11)} = \frac{\eta\left(11\eta^2-10\eta+3\right)}{18(\eta-1)^3(3\eta-1)^3} \tag{B31}$$

$$\mathbb{C}^{023}_{(s=11)} = \frac{\eta\left[\left(116\eta^4+40\eta^3-72\eta^2+6\eta\right)\tau_1+\left(174\eta^4+12\eta^3-95\eta^2+8\eta+9\right)\tau_3\right]}{36(\eta-1)^3(2\eta+1)^2(3\eta-1)^3} \tag{B32}$$

$$\mathbb{C}^{031}_{(s=11)} = -\frac{\left(388\eta^4-180\eta^3-118\eta^2+104\eta-24\right)\tau_1+\left(136\eta^4-45\eta^3-52\eta^2+37\eta-12\right)\tau_3}{108(\eta-1)^3(2\eta+1)(3\eta-1)^3} \tag{B33}$$

$$\mathbb{C}^{032}_{(s=11)} = \frac{\eta\left[\left(428\eta^4+88\eta^3-260\eta^2+38\eta+12\right)\tau_1+\left(442\eta^4+68\eta^3-241\eta^2+4\eta+15\right)\tau_3\right]}{108(\eta-1)^3(2\eta+1)^2(3\eta-1)^3} \tag{B34}$$

$$\mathbb{C}^{033}_{(s=11)} = -\frac{\eta\left(17\eta^2-18\eta+5\right)}{18(\eta-1)^3(3\eta-1)^3}\,, \tag{B35}$$

$$\mathbb{C}^{110}_{(s=1)} = -\frac{\eta^2(2\eta-1)}{9(\eta-1)^3(3\eta-1)^3} \tag{B36}$$

$$\mathbb{C}^{120}_{(s=1)} = \frac{(\tau_1-\tau_3)\left[\left(1012\eta^5+32\eta^4-636\eta^3+174\eta^2+72\eta-48\right)\tau_1+\left(526\eta^5+8\eta^4-329\eta^3+92\eta^2+39\eta-24\right)\tau_3\right]}{108(\eta-1)^3(2\eta+1)^2(3\eta-1)^3} \tag{B37}$$

$$\mathbb{C}^{130}_{(s=1)} = \frac{\left(388\eta^4-180\eta^3-118\eta^2+104\eta-24\right)\tau_1+\left(136\eta^4-45\eta^3-52\eta^2+37\eta-12\right)\tau_3}{54(\eta-1)^3(2\eta+1)(3\eta-1)^3} \tag{B38}$$

$$\mathbb{C}^{210}_{(s=1)} = -\frac{(\tau_1-\tau_3)\left[\left(1452\eta^5+48\eta^4-772\eta^3+146\eta^2+104\eta-48\right)\tau_1+\left(818\eta^5+16\eta^4-427\eta^3+84\eta^2+61\eta-24\right)\tau_3\right]}{108(\eta-1)^3(2\eta+1)^2(3\eta-1)^3} \tag{B39}$$

$$\mathbb{C}^{220}_{(s=1)} = -\frac{\eta\left(11\eta^2-10\eta+3\right)}{9(\eta-1)^3(3\eta-1)^3} \tag{B40}$$

$$\mathbb{C}^{230}_{(s=1)} = \frac{\eta\left[\left(452\eta^4-8\eta^3-128\eta^2-46\eta+36\right)\tau_1+\left(454\eta^4-52\eta^3-175\eta^2+16\eta+45\right)\tau_3\right]}{108(\eta-1)^3(2\eta+1)^2(3\eta-1)^3} \tag{B41}$$

$$\mathbb{C}^{310}_{(s=1)} = -\frac{\left(252\eta^4-144\eta^3-90\eta^2+92\eta-24\right)\tau_1+\left(176\eta^4-81\eta^3-56\eta^2+49\eta-12\right)\tau_3}{54(\eta-1)^3(2\eta+1)(3\eta-1)^3} \tag{B42}$$

$$\mathbb{C}^{320}_{(s=1)} = \frac{\eta\left[\left(204\eta^4-24\eta^3-72\eta^2-2\eta+20\right)\tau_1+\left(98\eta^4+4\eta^3-29\eta^2-8\eta+7\right)\tau_3\right]}{36(\eta-1)^3(2\eta+1)^2(3\eta-1)^3} \tag{B43}$$

$$\mathbb{C}^{330}_{(s=1)} = -\frac{\eta^2(2\eta-1)}{9(\eta-1)^3(3\eta-1)^3}\,, \tag{B44}$$

$$\mathbb{C}^{101}_{(s=1)} = \frac{\eta\left(11\eta^2-10\eta+3\right)}{18(\eta-1)^3(3\eta-1)^3} \tag{B45}$$

$$\mathbb{C}^{102}_{(s=1)} = \frac{(\tau_1-\tau_3)\left[\left(624\eta^4-286\eta^3-178\eta^2+130\eta-24\right)\tau_1+\left(164\eta^4-71\eta^3-52\eta^2+47\eta-12\right)\tau_3\right]}{108(\eta-1)^3(2\eta+1)(3\eta-1)^3} \tag{B46}$$

$$\mathbb{C}^{103}_{(s=1)} = -\frac{\eta\left[\left(55\eta^2-50\eta+12\right)\tau_1+\left(56\eta^2-55\eta+15\right)\tau_3\right]}{27(\eta-1)^3(3\eta-1)^3} \tag{B47}$$

$$\mathbb{C}^{201}_{(s=1)} = \frac{(\tau_1-\tau_3)\left[\left(8\eta^4+2\eta^3+30\eta^2-54\eta+24\right)\tau_1+\left(-172\eta^4+91\eta^3+56\eta^2-51\eta+12\right)\tau_3\right]}{108(\eta-1)^3(2\eta+1)(3\eta-1)^3} \tag{B48}$$

$$\mathbb{C}^{202}_{(s=1)} = -\frac{\eta\left(17\eta^2-18\eta+5\right)}{18(\eta-1)^3(3\eta-1)^3} \tag{B49}$$

$$\mathbb{C}^{203}_{(s=1)} = -\frac{\left(388\eta^4-180\eta^3-118\eta^2+104\eta-24\right)\tau_1+\left(136\eta^4-45\eta^3-52\eta^2+37\eta-12\right)\tau_3}{108(\eta-1)^3(2\eta+1)(3\eta-1)^3} \tag{B50}$$

$$\mathbb{C}^{301}_{(s=1)} = -\frac{\eta\left[\left(20\eta^2-19\eta+5\right)\tau_1+\left(17\eta^2-16\eta+4\right)\tau_3\right]}{9(\eta-1)^3(3\eta-1)^3} \tag{B51}$$

$$\mathbb{C}^{302}_{(s=1)} = \frac{\left(252\eta^4-144\eta^3-90\eta^2+92\eta-24\right)\tau_1+\left(176\eta^4-81\eta^3-56\eta^2+49\eta-12\right)\tau_3}{108(\eta-1)^3(2\eta+1)(3\eta-1)^3} \tag{B52}$$

$$\mathbb{C}^{303}_{(s=1)} = \frac{\eta\left(21\eta^2-20\eta+5\right)}{18(\eta-1)^3(3\eta-1)^3}\,, \tag{B53}$$

$$\mathbb{C}^{011}_{(s=1)} = \frac{\eta\left(21\eta^2-20\eta+5\right)}{18(\eta-1)^3(3\eta-1)^3} \tag{B54}$$

$$\mathbb{C}^{012}_{(s=1)} = \frac{\eta(\tau_1-\tau_3)\left[\left(244\eta^4-16\eta^3-86\eta^2-2\eta+22\right)\tau_1+\left(58\eta^4-4\eta^3-15\eta^2-8\eta+5\right)\tau_3\right]}{108(\eta-1)^3(2\eta+1)^2(3\eta-1)^3} \tag{B55}$$

$$\mathbb{C}^{013}_{(s=1)} = -\frac{\eta\left[\left(20\eta^2-19\eta+5\right)\tau_1+\left(17\eta^2-16\eta+4\right)\tau_3\right]}{9(\eta-1)^3(3\eta-1)^3} \tag{B56}$$

$$\mathbb{C}^{021}_{(s=1)} = \frac{\eta(\tau_1-\tau_3)\left[\left(\left(276\eta^4-94\eta^2-6\eta+22\right)\tau_1+\left(26\eta^4-20\eta^3-7\eta^2-4\eta+5\right)\tau_3\right]}{108(\eta-1)^3(2\eta+1)^2(3\eta-1)^3} \tag{B57}$$

$$\mathbb{C}^{022}_{(s=1)} = -\frac{\eta\left(17\eta^2-18\eta+5\right)}{18(\eta-1)^3(3\eta-1)^3} \tag{B58}$$

$$\mathbb{C}^{023}_{(s=1)} = \frac{\eta\left[\left(428\eta^4+88\eta^3-260\eta^2+38\eta+12\right)\tau_1+\left(442\eta^4+68\eta^3-241\eta^2+4\eta+15\right)\tau_3\right]}{108(\eta-1)^3(2\eta+1)^2(3\eta-1)^3} \tag{B59}$$

$$\mathbb{C}^{031}_{(s=1)} = -\frac{\eta\left[\left(55\eta^2-50\eta+12\right)\tau_1+\left(56\eta^2-55\eta+15\right)\tau_3\right]}{27(\eta-1)^3(3\eta-1)^3} \tag{B60}$$

$$\mathbb{C}^{032}_{(s=1)} = \frac{\eta\left[\left(116\eta^4+40\eta^3-72\eta^2+6\eta\right)\tau_1+\left(174\eta^4+12\eta^3-95\eta^2+8\eta+9\right)\tau_3\right]}{36(\eta-1)^3(2\eta+1)^2(3\eta-1)^3} \tag{B61}$$

$$\mathbb{C}^{033}_{(s=1)} = \frac{\eta\left(11\eta^2-10\eta+3\right)}{18(\eta-1)^3(3\eta-1)^3}\,. \tag{B62}$$

[1] A. Kitaev, Ann. Phys. **321**, 2 (2006).
[2] S. Trebst and C. Hickey, Phys. Rep. **950**, 1 (2022).
[3] S. M. Winter, A. A. Tsirlin, M. Daghofer, J. van den Brink, Y. Singh, P. Gegenwart, and R. Valentí, J. Phys.: Condens. Matter **29**, 493002 (2017).
[4] H. Takagi, T. Takayama, G. Jackeli, G. Khaliullin, and S. E. Nagler, Nat. Rev. Phys. **1**, 264 (2019).
[5] M. Hermanns, I. Kimchi, and J. Knolle, Annu. Rev. Con-

dens. Matt. Phys. **9**, 17 (2018).
[6] Y. Motome and J. Nasu, J. Phys.l Soc. Jpn. **89**, 012002 (2020).
[7] G. Jackeli and G. Khaliullin, Phys. Rev. Lett. **102**, 017205 (2009).
[8] K. W. Plumb, J. P. Clancy, L. J. Sandilands, V. V. Shankar, Y. F. Hu, K. S. Burch, H.-Y. Kee, and Y.-J. Kim, Phys. Rev. B **90**, 041112 (2014).
[9] L. J. Sandilands, Y. Tian, K. W. Plumb, Y.-J. Kim, and K. S. Burch, Phys. Rev. Lett. **114**, 147201 (2015).
[10] A. Banerjee, C. A. Bridges, J. Q. Yan, A. A. Aczel, L. Li, M. B. Stone, G. E. Granroth, M. D. Lumsden, Y. Yiu, J. Knolle, S. Bhattacharjee, D. L. Kovrizhin, R. Moessner, D. A. Tennant, D. G. Mandrus, and S. E. Nagler, Nature Materials **15**, 733 (2016).
[11] S.-H. Baek, S.-H. Do, K.-Y. Choi, Y. S. Kwon, A. U. B. Wolter, S. Nishimoto, J. van den Brink, and B. Büchner, Phys. Rev. Lett. **119**, 037201 (2017).
[12] Y. Kasahara, T. Ohnishi, Y. Mizukami, O. Tanaka, S. Ma, K. Sugii, N. Kurita, H. Tanaka, J. Nasu, Y. Motome, and et al., Nature **559**, 227 (2018).
[13] T. Yokoi, S. Ma, Y. Kasahara, S. Kasahara, T. Shibauchi, N. Kurita, H. Tanaka, J. Nasu, Y. Motome, C. Hickey, S. Trebst, and Y. Matsuda, Science **373**, 568 (2021).
[14] P. Czajka, T. Gao, M. Hirschberger, P. Lampen-Kelley, A. Banerjee, N. Quirk, D. G. Mandrus, S. E. Nagler, and N. P. Ong, Nature Materials **22**, 36 (2022).
[15] J. A. N. Bruin, R. R. Claus, Y. Matsumoto, N. Kurita, H. Tanaka, and H. Takagi, Nature Physics **18**, 401 (2022).
[16] T. Cookmeyer and J. E. Moore, Phys. Rev. B **98**, 060412 (2018).
[17] L. E. Chern, E. Z. Zhang, and Y. B. Kim, Phys. Rev. Lett. **126**, 147201 (2021).
[18] J. Feldmeier, W. Natori, M. Knap, and J. Knolle, Phys. Rev. B **102**, 134423 (2020).
[19] E. J. König, M. T. Randeria, and B. Jäck, Phys. Rev. Lett. **125**, 267206 (2020).
[20] M. Carrega, I. J. Vera-Marun, and A. Principi, Phys. Rev. B **102**, 085412 (2020).
[21] M. Udagawa, S. Takayoshi, and T. Oka, Phys. Rev. Lett. **126**, 127201 (2021).
[22] T. Bauer, L. R. D. Freitas, R. G. Pereira, and R. Egger, Phys. Rev. B **107**, 054432 (2023).
[23] D. Aasen, R. S. Mong, B. M. Hunt, D. Mandrus, and J. Alicea, Physical Review X **10** (2020).
[24] G. B. Halász, Gate-controlled anyon generation and detection in Kitaev spin liquids (2023), arXiv:2308.05154 [cond-mat.str-el].
[25] R. G. Pereira and R. Egger, Phys. Rev. Lett. **125**, 227202 (2020).
[26] S. Banerjee and S.-Z. Lin, SciPost Phys. **14**, 127 (2023).
[27] L. N. Bulaevskii, C. D. Batista, M. V. Mostovoy, and D. I. Khomskii, Phys. Rev. B **78**, 024402 (2008).
[28] D. I. Khomskii, J. Phys.: Condens. Matter **22**, 164209 (2010).
[29] S.-H. Jang, Y. Kato, and Y. Motome, Phys. Rev. B **104**, 085142 (2021).
[30] J. G. Rau, E. K.-H. Lee, and H.-Y. Kee, Phys. Rev. Lett. **112**, 077204 (2014).
[31] J. Knolle, S. Bhattacharjee, and R. Moessner, Phys. Rev. B **97**, 134432 (2018).
[32] S. Liang, M.-H. Jiang, W. Chen, J.-X. Li, and Q.-H. Wang, Phys. Rev. B **98**, 054433 (2018).
[33] J. Nasu, Y. Kato, Y. Kamiya, and Y. Motome, Phys. Rev. B **98**, 060416 (2018).
[34] M. Gohlke, G. Wachtel, Y. Yamaji, F. Pollmann, and Y. B. Kim, Phys. Rev. B **97**, 075126 (2018).
[35] A. Go, J. Jung, and E.-G. Moon, Phys. Rev. Lett. **122**, 147203 (2019).
[36] A. Ralko and J. Merino, Phys. Rev. Lett. **124**, 217203 (2020).
[37] H. Li, Y. B. Kim, and H.-Y. Kee, Phys. Rev. B **105**, 245142 (2022).
[38] F. Y ılmaz, A. P. Kampf, and S. K. Yip, Phys. Rev. Res. **4**, 043024 (2022).
[39] T. Cookmeyer and J. E. Moore, Phys. Rev. B **107**, 224428 (2023).
[40] A. Catuneanu, Y. Yamaji, G. Wachtel, Y. B. Kim, and H.-Y. Kee, npj Quantum Materials **3**, 23 (2018).
[41] J. S. Gordon, A. Catuneanu, E. S. Sørensen, and H.-Y. Kee, Nat. Commun. **10**, 2470 (2019).
[42] J. Wang, B. Normand, and Z.-X. Liu, Phys. Rev. Lett. **123**, 197201 (2019).
[43] S. M. Winter, Y. Li, H. O. Jeschke, and R. Valentí, Phys. Rev. B **93**, 214431 (2016).
[44] J. Fu, J. Knolle, and N. B. Perkins, Phys. Rev. B **97**, 115142 (2018).
[45] U. F. P. Seifert, T. Meng, and M. Vojta, Phys. Rev. B **97**, 085118 (2018).
[46] S.-S. Zhang, G. B. Halász, and C. D. Batista, Nat. Commun. **13**, 399 (2022).
[47] Z. Zhu, I. Kimchi, D. N. Sheng, and L. Fu, Phys. Rev. B **97**, 241110 (2018).
[48] C. Hickey and S. Trebst, Nature Communications **10**, 530 (2019).
[49] J. c. v. Chaloupka and G. Khaliullin, Phys. Rev. B **92**, 024413 (2015).
[50] S.-S. Zhang, G. B. Halász, W. Zhu, and C. D. Batista, Phys. Rev. B **104**, 014411 (2021).
[51] A. P. Joy and A. Rosch, Phys. Rev. X **12**, 041004 (2022).
[52] C. Wagner, M. F. B. Green, M. Maiworm, P. Leinen, T. Esat, N. Ferri, N. Friedrich, R. Findeisen, A. Tkatchenko, R. Temirov, and F. S. Tautz, Nature Materials **18**, 853 (2019).
[53] K. Bian, C. Gerber, A. J. Heinrich, D. J. Müller, S. Scheuring, and Y. Jiang, Nature Reviews Methods Primers **1**, 36 (2021).